Available online at www.sciencedirect.com
SCIENCE DIRECT®
International Journal of Heat and Mass Transfer 48 (2005) 3151–3166
International Journal of HEAT and MASS TRANSFER
www.elsevier.com/locate/ijhmt

Ventilation rates of micro-climate air annulus of the clothing-skin system under periodic motion

N. Ghaddar [a,*], K. Ghali [b], J. Harathani [a], E. Jaroudi [a]

[a] Department of Mechanical Engineering, American University of Beirut, P.O. Box 11-0236, Beirut 1107-2020, Lebanon
[b] Department of Mechanical Engineering, Beirut Arab University, Beirut, Lebanon

Received 24 August 2004; received in revised form 4 February 2005
Available online 14 April 2005

Abstract

A novel three-dimensional dynamic model is developed from first principles of mass and energy conservation of the modulated internal airflow in the variable annulus size between the clothing and the skin surface in presence of clothing apertures. The developed model solves for the flow and heat transfer problem in a finite length cylindrical annulus where the inner cylinder is oscillating within an outer fixed cylinder of porous fabric boundary. The changing annulus size induces pressure variations that cause air flow in the angular and the radial directions. In addition, axial airflow is present due to clothing open aperture to the atmosphere at one end of the annulus (sleeve or neck opening). The axial and angular flows in the trapped air layer are assumed locally governed by Womersley solution of time-periodic laminar flow in a plane channel in each direction. The 3-D model predicted the ventilation radial airflow through the fabric, the angular and axial airflow induced by the motion of the inner cylinder, and the sensible and latent heat losses from the skin due to ventilation with the presence of an open or closed aperture. Experiments were conducted using tracer gas method to measure time and space-averaged air ventilation rates induced by inner cylinder periodic motion within a fabric cylindrical sleeve at spacing amplitude ratio with respect to the mean of 0.8 for both closed and open aperture cases.

The ventilation rates within the annulus predicted by the 3-D model agreed well with experimental data at higher frequencies. For closed aperture situation at an amplitude ratio of 0.8, the mean percentage errors of the measurements compared with the predicted values of the model were 52%, 27.5% and 6.7% corresponding to the frequencies of 30 rpm, 40 rpm, and 60 rpm, respectively. Measured ventilation rates for open aperture agreed well with predicted ventilation rates at high frequencies giving lower values of total air renewal than the closed aperture results where the measured reductions in total ventilation rate compared to closed aperture were 8.5% and 14.3% corresponding to the frequencies of 40 rpm and 60 rpm, respectively. In addition, the model results showed that under walking conditions, a permeable clothing system with an open aperture reduced the heat loss from the skin by less than 1% when compared to the closed aperture clothing system. These results are consistent with previously published empirical data on air layer resistance for open and closed aperture of high air permeable fabric.

Keywords: Clothing ventilation model; Modulated microclimate air layer; Womersley flow; Steady periodic heat transfer in clothing

* Corresponding author. Tel.: +961 1 350000x3594/3590; fax: +961 1 744 462.
E-mail address: farah@aub.edu.lb (N. Ghaddar).
URL: http://webfaculty.aub.edu.lb/~farah/ (N. Ghaddar).

0017-9310/$ - see front matter © 2005 Elsevier Ltd. All rights reserved.
doi:10.1016/j.ijheatmasstransfer.2005.03.001

Nomenclature

A_f	area of the fabric (m^2)
C	specific heat (J/kg K)
C_D	dimensionless flow discharge coefficient at the aperture
D	water vapor diffusion coefficient in air (m^2/s)
e_f	fabric thickness (m)
f	frequency of oscillation of the fabric boundary (ventilation frequency) in rpm
h_{fg}	heat of vaporization of water (J/kg)
h_{ad}	heat of adsorption (J/kg)
H_{ci}	conduction heat transfer coefficient between inner node and outer node ($W/m^2 K$)
H_{co}	convection heat transfer coefficient between outer node and air flowing through fabric ($W/m^2 K$)
$h_{c(skin-air)}$	heat transport coefficient from the skin to the trapped air layer ($W/m^2 K$)
H_{mi}	diffusion mass transfer coefficient between inner node and outer node ($kg/m^2 kPa s$)
H_{mo}	mass transport coefficient between outer node and air void in the fabric ($kg/m^2 kPa s$)
$h_{m(skin-air)}$	mass transfer coefficient between the skin and the air layer ($kg/m^2 kPa s$)
k_a	thermal conductivity of air (W/m K)
L	fabric length in x direction (m)
$\dot{m}_{ax}$	mass flow rate of air in x-direction ($kg/m^2 s$)
$\dot{m}_{ay}$	mass flow rate of air in y-direction ($kg/m^2 s$)
$\dot{m}_{a\theta}$	mass flow rate of air in θ-direction ($kg/m^2 s$)
P_a	air vapor pressure (kPa)
P_i	vapor pressure of water vapor adsorbed in inner node (kPa)
P_o	vapor pressure of water vapor adsorbed in outer node (kPa)
R	total regain in fabric (kg of adsorbed H_2O/kg fiber)
R_v	water vapor gas constant (=0.461 kJ/kg K)
RH	relative humidity (%)
t	time (s)
T	temperature (°C)
w	humidity ratio (kg of water/kg of air)
W_o	Womersley number ($W_o = (Y/2)\sqrt{\omega/2v}$)
x	x-coordinate in the parallel direction to the fabric and skin
Y	instantaneous air layer thickness (m)
Y_m	mean air layer thickness (m)
y	y-direction

Greek symbols

ε	fabric emissivity
Φ	periodic dimensionless flow rate parameter in x-direction
ρ	mass density of fabric (kg/m^3)
ω	angular frequency (rad/s)
Λ_x	pressure gradient parameter in x-direction ($Pa m^2/kg$)
Λ_θ	pressure gradient parameter in θ-direction ($Pa m^2/kg$)
α	fabric air permeability ($cm^3/cm^2 s$)
v	*kinematic* air viscosity (m^2/s)
τ	period of the oscillatory motion (s)
σ	Stefan Boltzman constant = 5.669×10^{-8} $W/m^2 K^4$

Subscripts

a	conditions of air in the spacing between skin and fabric
i	inner node
o	outer node
sk	conditions at the skin surface
void	local air inside the void
∞	environment condition

1. Introduction

For the past two decades, the so-called pumping or bellows effect has been studied, and its importance on the heat and mass transfer of the human body has often been discussed [1–6]. In order to describe the dynamic behavior, Jones et al. [7,8] described a model of the transient response of clothing systems, which took into account the sorption behavior of fibers, but assumed local thermal equilibrium with the surrounding air. Li and Holcombe developed a mathematical model in which a human thermoregulatory model was combined with a kinetic sorption model of fabrics to study the transient thermal response of a clothed human [9]. Their model however neglected ventilation effects between the air passing through the fiber and the solid fiber. Ghali et al. [10] studied the effect of ventilation on heat and mass transport through a fibrous material to predict the transfer coefficients in a cotton fibrous medium. In realistic applications, ventilation of the clothing system during the human motion occurs by periodic motion of air in and out of the air spacing as the fabric moves outward or inward towards the skin. Ghali et al. [11] developed a model and reported experimental data on sensible and latent heat transport initiated by sinusoidal motion of a fabric plane above a sweating isothermal hot plate placed in a controlled environment. Their transient model predicted the heat loss from the wet boundary

and agreed fairly well with the experimentally measured values.

Previous periodic ventilation models of fibrous media of Lotens and Ghali et al. considered the impact of normal airflow [3,11,12]. However, Lotens's model was based on empirical equations that restricted its use. Ghali et al. normal periodic ventilation model is valid for normal airflow through the fabric, but is not applicable for parts of the body where there is a parallel airflow to the fabric at the sleeve and neck openings to the environment. A two-dimensional model was further developed by Ghali et al. [13] where parallel airflow to the fabric was present due to open apertures in clothed arms (sleeve end) or trunk (neck opening) using a locally fully-developed Poiseuille model for the flow in the parallel direction. The reported reduction in sensible and latent heat loss of the Poiseuille flow model of Ghali et al. [13] due to open aperture did not agree well with published experimental results of Lotens [3]. Ghali et al. [13] neglected the fluid inertia associated with the flow modulation and complete reversal during the flow cycle in the parallel direction and hence rendered the model applicability to low Womersley number ($W_o = (Y/2)\sqrt{\omega/2\nu}$) where ω is the ventilation circular frequency, Y is the air layer thickness, and ν is the air kinematic viscosity. Ghaddar et al. [2] extended the 2-D model of Ghali et al. [13] of skin-air-layer-fabric system to any frequency by taking into consideration the inertia effects of modulated parallel air layer flow. The flow is assumed to be locally governed by Womersley solution of time-periodic laminar flow in a plane channel [2,14,15]. The Ghaddar et al. model has predicted for parallel flow a lower flow rate in the axial direction when taking inertia due to airflow reversal into consideration compared to the Poiseuille flow model [2].

In real application, three-dimensional motion of trapped air exists between the cylindrical shaped body parts and the surrounding clothing. Air motion and flow will also take place in the angular direction and hence reduce further the radial flow rate in and out of the fabric due to gap height asymmetry. The first objective of this work is to develop from first principles a realistic 3-D model that can be used to predict air exchange rates within the internal air layer of a walking human at any speed in a loose-fitting one-layer ensemble with the clothing apertures open and closed. The model will predict the ventilation radial airflow, angular, and axial airflow induced by the motion of the inner cylinder and for closed and open aperture clothing. The model will also predict the skin heat and moisture transport resulting from the periodic motion of fabric with respect to the skin during walking. The second objective of the work is to experimentally validate the time-periodic averaged ventilation rates predicted by the developed 3-D theoretical model using trace gas method [6]. The contribution of this work is in the novel approach to modeling of the modulated internal air layer flow and transport process from first principles of mass and energy conservation while incorporating the Womersley flow model [2] in the angular and axial directions.

2. Model mathematical formulation

Fig. 1 depicts the schematic of the physical domain of the air-layer-fabric system where an enclosed air layer annulus of thickness Y and length L separates the fabric boundary and the human skin. The physical domain of the air-layer-fabric system represents a situation where skin is represented by a cylindrical solid impermeable surface covered with an outer clothing cylinder with one tight end (no air flow escapes from the annulus) and the other end is open to the atmosphere such as loose clothing openings at the sleeves end or around the neck. The skin inner boundary is assumed to have a sinusoidal up and down motion that induces air movement through the fabric. The flow of air is axial through the clothing openings (sleeves, skirts, neck), normal (radial) through air spaces within the clothing void spaces, and angular around the body segments such as arms, legs, and trunk. The radial airflow will be induced through the fabric material based on the pressure difference between the internal air layer pressure and that of the environment. The air flow in the axial direction x has a smaller pressure head loss compared with the flow through the fabric layer, and hence it is expected to result in a significant flow rate. The air flow in the angular direction will be governed by pressure differential due to variation of the internal air gap length $Y(\theta,t)$ that will drive the flow in θ-direction. The flow will be modeled as a flow between eccentric cylinders, where the flow in the narrow gap between the fixed outer cylinder (fabric) of radius R_f and a slightly smaller, off-set, inner cylinder (skin) of radius R_s moving up and down in sinusoidal motion. The eccentricity e_c of the cylinders is time dependent and relates directly to the oscillation frequency ω and amplitude ΔY by

$$e_c = \Delta Y \sin(\omega t) \tag{1}$$

Some elementary geometry shows that the width of the gap width Y between the two circular cylinders can be approximated by

$$Y(\theta, t) = Y_m - \Delta Y \sin(\omega t)\cos(\theta) \tag{2}$$

where Y_m represents the mean spacing between the human segment cylinder and the fabric outer cylinder ($Y_m = R_f - R_s$). The sinusoidal motion is an approximate model of the periodic change of air spacing layer thickness for a walking person. Human gait analysis show repeated periodic pattern of limbs motion as a function of walking speed that can be approximated as a sinusoidal pattern [16]. One end of the air layer

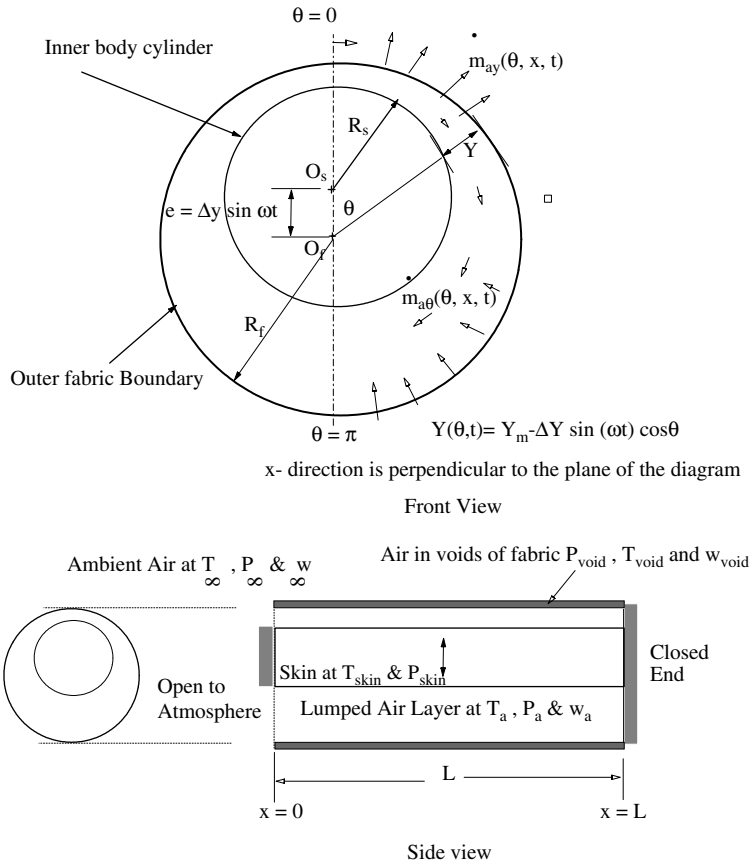

Fig. 1. Schematic of the physical domain of the fabric-air layer-skin system, the fabric model.

physical domain at $x = 0$ is open to ambient air resembling the presence of a clothing open aperture and the other end at $x = L$ is impermeable to flow (closed). The fabric thickness is e_f. The frequency of the oscillating motion of the fabric is generally proportional to the activity level of the walking human. The air spacing layer beneath the fabric will be formulated as an incompressible layer. The induced flow (during walking) in the axial direction exhibits periodic motion with complete reversal for flow from the atmosphere into the domain through the aperture during the fabric upward motion and out of the domain to the atmosphere during the fabric downward motion. The flow inertia associated with high modulation rates of the air cannot be neglected.

In this section, the formulation of the periodic ventilation problem in presence of an open aperture addresses the radial (normal) air flow through the outer fabric boundary using the three-node fabric model [1,2]; and the modeling of the internal air layer motion and transport processes while accounting for the flow inertia in the axial and angular directions due to the periodic motion and flow reversal during the walking cycle.

2.1. Air flow mass balance

The flow inertia due to periodic oscillation of air in and out of the open aperture induced by the inner cylinder up and down motion will be accounted for by assuming the flow to be locally a Womersley steady-periodic flow. Similarly, the angular flow in the annulus exhibits periodic motion toward the direction of increasing gap thickness within the periodic motion. The radial airflow passing through the fabric layer during ventilation has also an obvious significant effect on the heat and mass transport at the fabric and from the skin. A general air layer mass balance performed on an element of height Y, thickness $R_f d\theta$, and depth dx is given by

$$\frac{\partial(\rho_a Y)}{\partial t} = -\dot{m}_{ay} - \frac{\partial(Y\dot{m}_{ax})}{\partial x} - \frac{\partial(Y\dot{m}_{a\theta})}{R_f \partial\theta} \tag{3}$$

where $\dot{m}_{ax}$ is the mass flux in the axial direction in kg/m^{2}s, $\dot{m}_{a\theta}$ is the mass flux in the angular direction, and $\dot{m}_{ay}$ is the radial air flow rate. The boundary conditions for the air flow are

$$\dot{m}_{ax}(x=0,\theta)=0 \tag{4a}$$

$$\dot{m}_{ax}(x=L,\theta)=C_D\left[\frac{2\rho_a}{|P_L-P_\infty|}\right]^{\frac{1}{2}}[P_\infty-P_L] \tag{4b}$$

$$\dot{m}_{a\theta}(x,\theta=0)=0 \tag{4c}$$

$$\dot{m}_{a\theta}(x,\theta=\pi)=0 \tag{4d}$$

where Eq. (4b) is derived from the pressure drop at the opening by applying Bernoulli's equation from P_∞ in the far environment ($x\to-\infty$) to the opening at $x=0$, and C_D is the discharge loss coefficient at the aperture of the domain dependent on discharge area ratio of the aperture to the air layer thickness Y. The mass flow rate in θ and x directions will be solved in terms of the driving pressure gradient in each direction, while the flow rate in radial direction is governed by the pressure differential across the fabric between the local air layer pressure and the atmospheric pressure and depends on the permeability of the fabric material.

2.2. Modeling of the radial air flow normal to the fabric

The analysis of the airflow through the fabric boundary of the physical domain depicted in Fig. 1 is based on the single lumped fabric layer of three-node adsorption model described in detail by Ghali et al. [1,11]. In summary, the three-node model lumps the fabric into an outer node, inner node, and an air void node. The air flowing through the fabric void spaces does not spend sufficient time to be in thermal equilibrium with the fabric inner and outer nodes. The moisture uptake in the fabric occurs first by the convection effect from the air in the void node to the yarn surface (outer node), followed by sorption/diffusion to the yarn interior (inner node). The mass and energy balances of the fabric three-node model are found in detail in Ref. [1] and will not be repeated here. The modified fabric internal transport coefficients of Ghaddar et al. [2] are used in this work to extend the applicability of the normal ventilation model to low normal flow rates that will occur near the openings.

In this study the permeability of the fabric is considered constant at the standard experimentally measured value under the pressure difference $\Delta P_m = 0.1245$ kPa [17]. To get the normal airflow passing through the fabric at other pressure differentials, other than the 0.1245 kPa, the amount of airflow is proportional to the pressure differentials [1]. The normal airflow rate is then represented by

$$\dot{m}_{ay}=\frac{\alpha\rho_a}{\Delta P_m}(P-P_\infty)\quad \mathrm{kg/m^2\,s} \tag{5}$$

where α is the fabric air permeability ($\alpha = 4.99$ cm^3/cm^2 s), and, P is the air pressure of the air layer between the skin and the fabric and P_∞ is the outside environment air pressure.

2.3. Modeling of the axial and angular internal air layer flows

The flow in the x-direction, driven by time-periodic pressure gradient, will be treated as locally governed by Womersley time-periodic laminar channel base flow [14,15,18]. Given oscillatory flow of the air, Womersley further simplifies the analysis by assuming the channel to be of sufficient length such that the flow is fully-developed and the slope $\partial Y/(R_f\partial\theta)$ is small to allow quasi-parallel flow in the angular direction within the annulus. With these simplifications, the governing momentum equation for the axial velocity at any position x at fixed θ and the momentum equation for the angular velocity at any position θ at fixed x, respectively become

$$\frac{\partial u_x}{\partial t}=-\frac{1}{\rho_a}\frac{\partial P}{\partial x}+\nu\frac{\partial^2 u_x}{\partial y^2} \tag{6a}$$

$$\frac{\partial u_\theta}{\partial t}=-\frac{1}{\rho_a R_f}\frac{\partial P}{\partial \theta}+\nu\frac{\partial^2 u_\theta}{\partial y^2} \tag{6b}$$

The driving pressure in the air layer is oscillating with the same frequency of the inner cylinder motion but with a phase difference of (π/2). At the minimum spacing position $Y_{min} = Y_m - \Delta Y$ and the maximum spacing position $Y_{max} = Y_m + \Delta Y$, the pressure in the air layer equalizes with P_∞ before the radial flow changes direction. The driving pressure gradients in the axial and angular directions are written as follows:

$$-\frac{1}{\rho_a}\frac{\partial P}{\partial x}=\Lambda_x\sin\left(\omega t+\frac{\pi}{2}\right)=\Lambda_x\cos(\omega t) \tag{7a}$$

$$-\frac{1}{\rho_a R_f}\frac{\partial P}{\partial \theta}=\Lambda_\theta\sin\left(\omega t+\frac{\pi}{2}\right)=\Lambda_\theta\cos(\omega t) \tag{7b}$$

where Λ_x is the pressure gradient amplitude factor (Pa m^2 kg^{-1}) and Λ_θ is the pressure gradient amplitude factor in the angular direction (Pa m^2 kg^{-1}). Both amplitude factors, Λ_x and Λ_θ will be adjusted to satisfy the air layer mass balance. Assuming a frequency-separable transient solution, Eq. (6) are written for an oscillating laminar flow in a channel for x and θ directions as follows:

$$\frac{\partial u_x}{\partial t}=\Lambda_x\cos(\omega t)+\nu\frac{\partial^2 u_x}{\partial y^2}\quad\text{and}\quad u_x\left(\pm\frac{Y}{2},t\right)=0 \tag{8a}$$

$$\frac{\partial u_\theta}{\partial t}=\Lambda_\theta\cos(\omega t)+\nu\frac{\partial^2 u_\theta}{\partial y^2}\quad\text{and}\quad u_\theta\left(\pm\frac{Y}{2},\theta,t\right)=0 \tag{8b}$$

The analytical solution of Eqs. (8a) and (8b) exists in literature for $u_x(y,t)$ and similarly $u_\theta(x,t)$ as reported by

Straatman et al. [18] in dimensionless form for $u'_x(y,t) = u_x(y,t)/(\Lambda_x/\omega)$ and $u'_\theta(x,t) = u_\theta(y,t)/(\Lambda_\theta/\omega)$. The dimensionless axial and similarly angular velocities are expressed as a function of y, t and the physical parameters ω and ν [18]. The velocities in both directions differ only in the amplitude factor of the driving pressure gradient Λ_x and Λ_θ. By prescribing a flow condition such as pressure or volume flow rate in either direction, with the same ventilation frequency, the value of Λ_x *and/or* Λ_θ can be determined at any given height Y. The mass flow rate per unit area can be calculated as a function of time at any local position x by integrating the x-velocity $u'_x(y,t)$ over the height analytically or numerically as:

$$\dot{m}'_{ax}(t) = \dot{m}_{ax} Y = \rho_a \frac{Y\Lambda_x}{2\omega}\Phi(t) \tag{9a}$$

where Φ is the dimensionless flow rate for a unit pressure gradient parameter given by

$$\Phi(t) = \int_{-1}^{1} u'_x(y',t)\,dy' \tag{9b}$$

Similarly, the angular mass flow rate at any local angular position θ is found by integrating u_θ over the layer spacing Y at that position as:

$$\dot{m}'_{a\theta} = \dot{m}_{a\theta}(t) Y = \rho_a \frac{Y\Lambda_\theta}{2\omega}\Phi(t), \quad (\mathrm{kg/sm}) \tag{10}$$

The air mass flow rate per unit depth $\dot{m}'_{ax}(t)$ is related to the pressure drop in the channel through Eq. (6). The pressure drop at the opening ($x = 0$) can be calculated by applying Bernoulli's equation from P_∞ in the far environment to the opening at $x = 0$. The flow rate per unit width in the angular direction has been related to the angular pressure gradient by combining the standard lubrication theory in fluid dynamics [19] and the Womersley flow in a channel. Since the mass flow rate is modeled as a function of pressure differences independently in r, θ, and x directions, then the mass balance of the air layer would result in the following pressure equation

$$\rho_a \frac{\partial Y}{\partial t} = -\gamma_{ay}(P_a - P_\infty) + \frac{Y\rho_a\Phi(t)}{2\omega}\frac{\partial \Lambda_x}{\partial x} + \frac{\rho_a\Phi(t)}{2\omega}\frac{\partial(Y\Lambda_\theta)}{R_f\partial\theta} \tag{11}$$

Eqs. (7) and (11) can be solved numerically for P_a, Λ_x and Λ_θ at any discrete location within the air layer as a function of time while satisfying the imposed boundary conditions given in Eqs. (4a)–(4d).

2.4. Water vapor mass balance

Once the pressure and mass flow rates in the air layer are determined, the water vapor mass balance is performed on the air layer. During the oscillation cycle, the air from the environment will move through the fabric void into the air layer when the pressure in the air layer $P_a(x,\theta)$ is less than that of the environment P_∞. The airflow into the air spacing layer coming from the air void node of the fabric will have the same humidity ratio as the air in the void space of the fabric. The water vapor mass balance for the air spacing layer when $P_a(x,\theta)$ is less than P_∞ is given by

$$\frac{\partial(\rho_a Y w_a)}{\partial t} = h_{m(\mathrm{skin-air})}[P_{sk} - P_a] - \dot{m}_{ay} w_{void} - \frac{\partial(Y\dot{m}_{ax} w_a)}{\partial x} - \frac{\partial(Y\dot{m}_{a\theta} w_a)}{R_f\partial\theta} + D\frac{\rho_a(w_{void} - w_a)}{e_f/2}, \quad P_a(x,\theta) < P_\infty \tag{12a}$$

When the pressure in the air layer $P_a(x,\theta)$ is greater than P_∞, the airflow through the fabric void out of the air spacing will carry the same humidity ratio of the internal air layer. Then the water vapor mass balance for the air spacing layer when $P_a(x,\theta)$ is greater than P_∞ is given by

$$\frac{\partial(\rho_a Y w_a)}{\partial t} = h_{m(\mathrm{skin-air})}[P_{sk} - P_a] - \dot{m}_{ay} w_a - \frac{\partial(Y\dot{m}_{ax} w_a)}{\partial x} - \frac{\partial(Y\dot{m}_{a\theta} w_a)}{R_f\partial\theta} + D\frac{\rho_a(w_{void} - w_a)}{e_f/2}, \quad P_a(x,\theta) > P_\infty \tag{12b}$$

where $h_{m(\mathrm{skin\text{-}air})}$ is the mass transfer coefficient between the skin and the air layer. The terms on the right hand side of Eqs. (12a) and (12b) are explained as follows: the first term represents the mass transfer from the skin to the trapped air layer where the mass transfer coefficient at the skin to the air layer is obtained from published experimental values of Ghaddar et al. [12]; the second term is the convective mass flow coming through the fabric voids; the third term represents the net flux in the axial direction; the fourth term is the net flux in the angular direction and the last term is the water vapor diffusion term from the air layer to the air in the fabric void due to the difference in water vapor concentration.

2.5. Energy balance of the air layer

The energy balance for the air–vapor mixture in the air spacing layer will be performed taking into account the axial and angular air motions, as well as the radial motion with its effect on the properties of the air mass that enters the domain and leaves the domain during the oscillatory upward and downward motion of the inner cylindrical boundary. An energy balance of the air spacing of the fabric expresses the rate of change of the energy air–vapor mixture of the air-layer in terms of the external work done by the environment on the air layer, the evaporative heat transfer from the moist skin, the dry convective heat transfer from the skin, the convection of heat to the air layer associated with $\dot{m}_{ay}$ coming through the fabric boundary, and the heat diffusion from void air to confined air layer due to gradients in temperature and water-vapor concentrations.

The energy balance of the air layer when $P_a(x,\theta)$ is less than P_∞ is given by

$$\begin{aligned}&\frac{\partial}{\partial t}\left[\rho_a Y(C_v T_a + w_a h_{fg})\right] + P_\infty \frac{\partial Y}{\partial t}\\ &= h_{m(skin-air)} h_{fg}[P_{sk} - P_a] + h_{c(skin-air)}[T_{sk} - T_a]\\ &\quad - \dot{m}_{ay}[C_p T_{void} + w_{void} h_{fg}] - \frac{\partial Y[\dot{m}_{ax}(C_p T_a + w_a h_{fg})]}{\partial x}\\ &\quad - \frac{\partial[Y\dot{m}_{a\theta}(C_p T_a + w_a h_{fg})]}{R_f \partial\theta} + D h_{fg}\frac{\rho_a(w_{void} - w_a)}{e_f/2}\\ &\quad + k_a\frac{(T_{void} - T_a)}{e_f/2},\\ &P_a(x,\theta) < P_\infty \end{aligned} \tag{13a}$$

When $P_a(x,\theta)$ is greater than P_∞, the energy balance in the air spacing layer becomes

$$\begin{aligned}&\frac{\partial}{\partial t}\left[\rho_a Y(C_v T_a + w_a h_{fg})\right] + P_\infty \frac{\partial Y}{\partial t}\\ &= h_{m(skin-air)} h_{fg}[P_{sk} - P_a] + h_{c(skin-air)}[T_{sk} - T_a]\\ &\quad - \dot{m}_{ay}[C_p T_a + w_a h_{fg}] - \frac{\partial[Y\dot{m}_{ax}(C_p T_a + w_a h_{fg})]}{\partial x}\\ &\quad + \frac{\partial[Y\dot{m}_{a\theta}(C_p T_a + w_a h_{fg})]}{R_f \partial\theta} + D h_{fg}\frac{\rho_a(w_{void} - w_a)}{e_f/2}\\ &\quad + k_a\frac{(T_{void} - T_a)}{e_f/2},\\ &P_a(x,\theta) > P_\infty \end{aligned} \tag{13b}$$

where k_a is the thermal conductivity of air since the fabric void thickness is very small, conduction of heat from the fabric void air to the trapped air layer is represented by the law of the wall as shown in the last two terms of Eqs. (13a) and (13b).

3. Numerical procedure

3.1. Discrete formulation

The control volume methodology is used to divide the air layer into grids of size Δx, $R_f\Delta\theta$, and height $Y(\theta,t)$ as shown in Fig. 2. Each grid volume contains a lumped adsorption system of fibrous inner, outer nodes and air void as the upper boundary. The discrete air pressure at the volume center and annulus gap size notations are

$$P^n_{i,j} = P_a(n\Delta t, (x_{i-1,j} + x_{i,j})/2, jR_f\Delta\theta) \tag{14a}$$

$$\begin{aligned}&Y^n_j = Y_m + \Delta Y \sin(\omega n\Delta t)\cos(j\Delta\theta),\\ &\{i = 0\ldots N_x, \text{ and } j = 0, N_\theta\}\end{aligned} \tag{14b}$$

where n is the discrete time step number.

In this work, only the discrete model equations for the air mass balance are given to illustrate the methodology. At the end boundary $x = 0$, there will be a flow direct to or from the environment, $\dot{m}_0$. The mass flow rates in x and θ directions are dependent on the pressure gradient parameters Λ_x, and Λ_θ, while $\dot{m}_{ay}$ depends on pressure difference $(P_a - P_\infty)$. The temporal integration

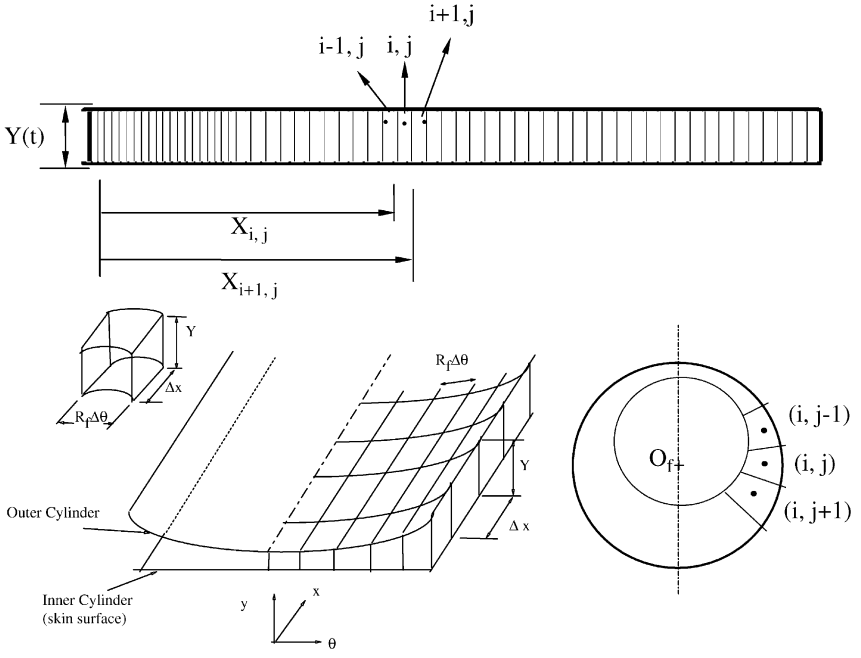

Fig. 2. The discrete system.

of the air layer mass balance for an internal node (i,j), assuming air is incompressible, is performed using the first order Euler Forward scheme. The discrete form of the air mass balance equation is given by

$$\rho_a\left(\frac{dY_j^n}{dt}\right)=\gamma_{ay}\left(P_\infty-P_{i,j}^n\right)-\rho_a\times\frac{Y_j^n}{2\omega}\Phi^n\left[\frac{\Lambda_{x(i,j)}^n-\Lambda_{x(i-1,j)}^n}{\Delta x}+\frac{\Lambda_{\theta(i,j)}^n-\Lambda_{\theta(i,j-1)}^n}{R_f\Delta\theta}\right]-\rho_a\frac{\Lambda_{\theta(i,j)}^n}{2\omega}\Phi^n\left[\frac{Y_{j+1}^n-Y_j^n}{R_f\Delta\theta}\right] \quad (15a)$$

where γ_{ay} is a linearized coefficient in the radial direction, kg/kPa s m^2 obtained from Eq. (4) as

$$\gamma_{ay}=\frac{\alpha\rho_a}{\Delta P_m} \quad (15b)$$

Eq. (15a) has three unknowns $P_{i,j}^n$, $\Lambda_{x(i,j)}$ and $\Lambda_{\theta(i,j)}$. The gradient factors $\Lambda_{x(i,j)}$ and $\Lambda_{\theta(i,j)}$ are correlated to the pressure by

$$P_{i+1,j}^n=P_{i,j}^n+\rho_a\Lambda_{x(i,j)}^n\Delta x\sin(\omega n\Delta t) \quad (16a)$$

$$P_{i,j+1}^n=P_{i,j}^n+\rho_a\Lambda_{\theta(i,j)}^n R_f\Delta\theta\sin(\omega n\Delta t) \quad (16b)$$

The above equations are solved at each time step for the pressure $P_{i,j}^n$, $\Lambda_{x(i,j)}^n$ and $\Lambda_{\theta(i,j)}^n$ at every node in the computational domain. The pressure is used to determine the airflow in each direction. The pressure and the airflow rates are then used as direct inputs in the water vapor mass balance and the energy balance of the air layer control volume, and of the fabric nodes and void space. These equations will be integrated numerically using first-order Euler-Forward scheme in time and control volume methodology in space.

The solution will start at each time step by assuming a value of the pressure at node (N_x, N_θ) calculating the pressure at the opening (see Eq. (4b)), solving the pressure equations for Λ_x and Λ_θ in Eqs. (15a) and (15b) concurrently with the pressure recurrence formula in Eq. (16) at all the internal nodes. The solution will produce new value of $P_{Nx,j}$ which will be used again in the solution of Eqs. (16a), (16b) and (15) until the solution converges where the percent error in the pressure between any two iterative steps is less than 10^{-7}%. Once the pressure distribution is determine at any time step, the mass flow rates in all directions are calculated and then the water vapor mass balances and the energy balances are solved for the values of temperature and humidity ratio of the air layer, and the fabric inner, outer and air void nodes. The vapor pressure of the flowing air in the air spacing layer or in the fabric voids is related to the air relative humidity, RH, and temperature and is calculated using the psychometric formulas of Hyland and Wexler [20] to predict the saturation water-vapor pressure and hence the vapor pressure at the specified relative humidity.

The evaluation of the instantaneous sensible and latent heat loss from the inner cylinder then follows. The mean steady periodic time and space-averaged values of the mass flow rates are also calculated. The normal ventilation rate integrated over one time period of motion at any axial position is defined by

$$\overline{\dot m_{aY}}=\frac{1}{\tau}\int_0^\tau\int_{-\pi/2}^{\pi/2}\dot m_{ay}R\,d\theta\,dt,\quad \text{kg/s m}^2 \quad (17a)$$

where τ is the period of oscillation. The net ventilation rate inflow or outflow to the microclimate air layer through the open aperture during one period of motion is defined by

$$\overline{\dot m_o}=\frac{1}{\tau}\int_0^\tau\int_{-\pi/2}^{\pi/2}\dot m_o\,d\theta\,dt\quad \text{kg/s m}^2 \quad (17b)$$

For the parametric analysis, a dimensionless amplitude parameter is introduced by

$$\zeta=\frac{\Delta Y}{Y_m}=\frac{\Delta Y}{R_f-R_s} \quad (17c)$$

where the maximum change in the annulus spacing is divided by the mean annulus spacing.

3.2. Numerical accuracy and stability

Numerical tests were performed to assure a grid independent, stable and accurate solution for a domain of length $L = 50$ cm, $R_f = 7.56$ cm, $R_s = 3.75$ cm, $C_D = 1$, $Y_m = 38.1$ mm and $\Delta Y = 0.635$ mm at $f = 25$ rpm using different mesh sizes to get a grid independent solution in axial and angular directions. Runs were performed with uniform grid sizes of $\Delta x = 0.01$ m, 0.005 m, and 0.004 m and a variable gird size of 0.005 close to opening and 0.01 for inner parts. The variable grid size produced grid independent results with less number of grid points than the uniform grid of the axial mass flow rate. In the polar direction, uniform values of $\Delta\theta = 6°$, 9°, 11.25°, and 18° degrees were used to test grid independent solution in that direction. At $\Delta\theta = 18°$ and 6°, the relative error is 0.8% at the maximum flow rate while the error for $\Delta\theta = 9°$ and 6° degrees is 0.0539%. The size of the time step was taken at 0.01 s and 0.001 s over a total integration period of 3600 s. At low frequencies, the higher time step of 0.01 was sufficient to produce a stable accurate solution with the selected grid size.

4. Experimental procedure for estimation of the ventilation rates

In this section, the developed experimental setup to measure the time-space averaged radial airflow rates renewal in the air layer for closed aperture system and total ventilation rate for open aperture system is

discussed. Experiments were conducted in a climatic chamber where temperature and humidity were maintained at $T_\infty = 25 \pm 0.5$ °C and RH = 50 ± 2%, respectively. Untreated cotton was chosen as a representative of a most common worn fabric to use in the ventilation tests. The cotton was obtained from Test fabrics Inc. (Middlesex, NJ 08846), and is made of unmercerized cotton duck, style #466 of thickness of 1 mm.

Fig. 3 shows a schematic of the experimental setup that consisted of: (i) a PVC solid inner cylinder (arm) 7.8 cm in diameter and 60 cm long; (ii) an outer 60 cm long cylinder (sleeve) of 13 cm diameter made of a thin metallic screen of 2 cm open squares where the cotton fabric is wrapped around and fitted; (iii) a power screw mechanism for up and down motion that includes, two power screws, two sliders, two guides, electric DC motor; relays for reversing motor direction of rotation; and chain drive; (iv) support platform; and (v) flexible impermeable plastic membranes. The selection of the length is based on realistic physical length of a sleeve, or cloth-covered trunk between the waist and the aperture at neck. The inner cylinder is connected to the sliders of the power screw mechanism where it is subjected to an up and down motion driven by the gear and chain mechanism connected to the DC motor. The DC motor rotational speed is controlled by a variable power supply to obtain different motion frequencies. The outer sleeve cylinder is fixed to the platform frame and is capped at both ends with a flexible impermeable plastic membrane to prevent air leaks in the axial direction. The periodic motion is not exactly a sinusoid where the inner cylinder moves up at constant speed to reach the maximum

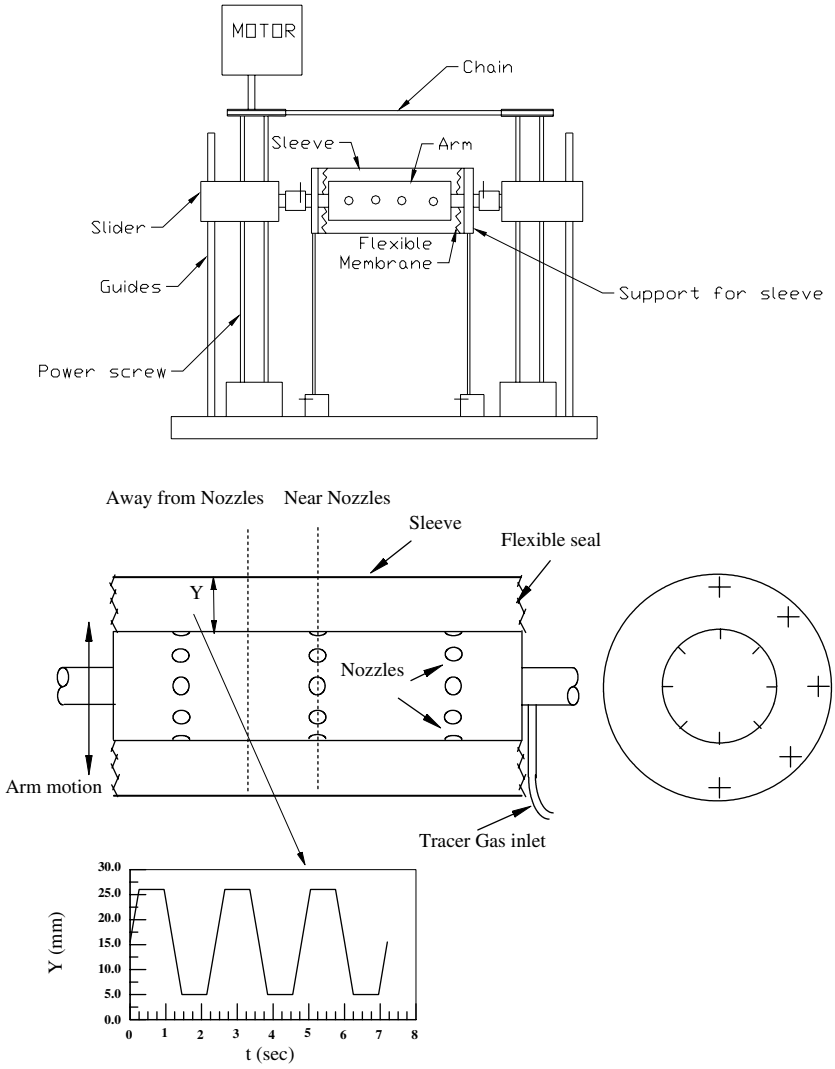

Fig. 3. Experimental setup.

height and then the relay reverses direction to start the downward motion of the cycle as shown in Fig. 3. The amplitude of oscillations tested is 21 mm corresponding to amplitude ratios of $\zeta = 0.8$. The selection of the amplitude of oscillation is selected to represent cases of medium to loose clothing situations. Experiments are conducted for gear motor frequencies of 30, 40 and 60 rpm. In the plane above the fabric cylinder, a fan is placed to provide sufficient circulation of air (0.7 m/s) for maintaining the constant chamber ambient conditions around the fabric.

The radial (normal to the fabric) time-space-averaged ventilation flow rate is measured using tracer gas method with both ends of the annulus closed. The radial air flow rate is induced by the inner cylinder motion at fixed environment temperature in the climatic chamber. The tracer gas method is used as described by Havenith et al. [6]. The measurements are done by injecting an inert gas (N_2) at a fixed rate through nozzles placed at holes drilled in the inner cylinder normal to the surface where the location of the holes drilled on the side and front views of the air annulus. The concentration of the oxygen gas is measured in the air gap at different angular and axial locations using a standard exhaust gas analyzer (Emissions Systems INC, EMS Model 4001). The gas analyzer measurements have an accuracy of ±0.05% of volume of O_2 of air sample. The concentration is measured at a radial distance of 4 mm in the air layer away from the fabric outer cylinder. The nitrogen gas is injected by a flow regulator that injects nitrogen into the air layer in the range of 0.1–1.5 L/min from a pressurized nitrogen vessel. The standard air sample composition by volume is 79% N_2 and 21% O_2. To obtain the concentration of N_2 in the microclimate, the recorded concentration of O_2 is deducted from the 100 %. The total volume flow rate renewal can be calculated from the trace gas mass flux ψ_{tr} (m^3/s), and the measured concentrations C_a (m^3 O_2/m^3 air) and C_∞ (m^3 O_2/m^3 air) at inner and outer locations, respectively, as:

$$\frac{\overline{\dot{m}_a}}{\rho_a}[C_\infty - C_a] + \psi_{tr} = 0 \tag{18}$$

The concentrations measured in the microclimate between the cylinder and the fabric cylindrical layer by direct sensor readings.

Two sets of experiments were conducted for the case of closed apertures at both ends of the annulus and the case of open aperture at one end. The experimental setup was placed in the environmental chamber where constant climatic conditions were maintained for a period of 24 h before the start of the experiments. At any selected frequency of the moving inner cylinder, the motion is maintained for at least 60 min before a steady injection of the N_2 through the holes of the inner cylinder was started. Steady conditions of renewal flow rate of the air in the annulus were reached within 0.5 h from the onset of injection. The reading of N_2 concentrations were recorded every 10 min for 1 h of the climatic chamber air outside the fabric sleeve and at three axial positions as shown in the figure and at five different angular locations inside the annulus of the air layer for both sets of closed and open aperture experiments at the three selected frequencies. The experiments were repeated at different N_2 injection rates to check the homogeneity of the calculated N_2 concentration inside the annulus and repeatability of the O_2 concentration measurements. A value of 0.5 L/min was selected to conduct the measurements. The environmental chamber air was refreshed frequently between experiments to prevent nitrogen concentration build up in the chamber. The air renewal rate in the annulus was calculated using Eq. (18).

5. Results and discussion

The ambient conditions for the simulations are taken for all the runs similar to the experimental conditions of 25 °C and 50% RH and the inner cylinder skin condition is taken as saturated at 35 °C and 100% relative humidity. First, a comparison is performed between experimental and numerical model predictions of ventilation rates. Results of the 2-D radial and angular flow are then presented for close apertures and results of the 3-D model are discussed when the system has an open aperture at $x = 0$. Comparison is made with the limiting cases of normal 1-D flow [1], 2-D plane flow [2], and to published empirical results of Lotens [3,21].

5.1. Experimental validation of the ventilation model

Fig. 4(a) and (b) shows a plot of the experimentally measured (a) radial mass ventilation rate $\bar{m}_{aY}$ of the closed apertures setting and (b) total ventilation rate ($\bar{m}_{aY} + \bar{m}_o$) of the open aperture at one end setting as a function of the frequency of oscillation at an amplitude ratio of $\zeta = 0.8$ for a domain length of 0.6 m. The theoretically predicted values are also shown on the same plot. The agreement of the model prediction improves significantly at higher frequencies. At $\zeta = 0.8$, the mean percent error of the measurements compared with the predicted values of the model were 52%, 27.5% and 6.7% corresponding to the frequencies of 30 rpm, 40 rpm, and 60 rpm, respectively. The large error at the low frequency of oscillation is due to the lower angular flow rate that decreases the homogeneity in the nitrogen concentration and would result in a larger error in the measured concentration average at the different angular positions. Good agreement was obtained between the model prediction and experimental measurements for open apertures where the mean percent errors of the measurements compared with the predicted values of

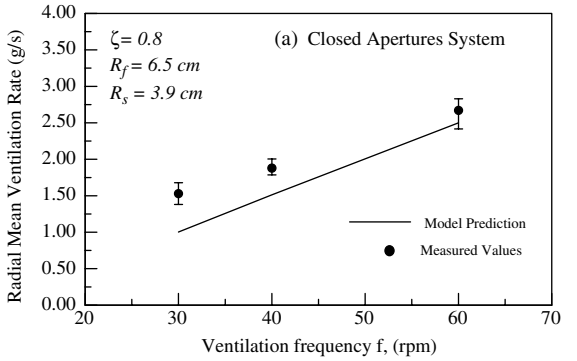

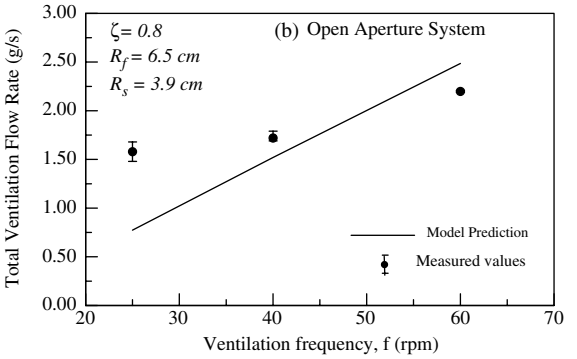

Fig. 4. (a,b) A plot of the experimentally measured (a) radial mass ventilation rate $\bar{m}_{aY}$ of the closed apertures setting and (b) total ventilation rate ($\bar{m}_{aY} + \bar{m}_o$) of the open aperture at one end setting as a function of the frequency of oscillation at an amplitude ratio of $\zeta = 0.8$ for a domain length of 0.6 m. The theoretically predicted values are also shown on the same plot.

the model were 51%, 11.6% and 13% corresponding to the frequencies of 25 rpm, 40 rpm, and 60 rpm, respectively. The total air renewal ventilation rates for open aperture are smaller than the closed aperture renewal values at the same frequency.

5.2. Closed apertures radial and angular flow system analysis (no axial flow)

Fig. 5(a)–(c) shows the angular variation of (a) the radial ventilation flux at $\zeta = 0.16$; (b) the radial ventilation flux at $\zeta = 0.8$; and (c) the angular internal flow at $\zeta = 0.8$ of the air in the annulus for different times in the motion cycle at $f = 25$ rpm, $Y_m = 38.1$ mm, $L = 50$ cm, $R_f = 7.56$ cm, $R_s = 3.75$ cm, and $C_D = 1$. As the amplitude increases, the ventilation flux in the radial direction increases. The position of zero radial mass flux deviates from $\theta = 90°$. This deviation increases with the increase of amplitude ratio. Due to symmetry, the angular air mass flux is zero at $\theta = 0$ and $\theta = 180°$. The position of the maximum mass flux in the angular direction changes with time. A vector plot of the radial and angular air layer mass fluxes is shown in Fig. 6 different times of the cycle with a step of 0.3 s = 0.125 t/τ at $\zeta = 0.8$ and $f = 25$ rpm. The air layer flow is zero when the inner cylinder reaches extreme positions up and down. The pressure within the air layer at those positions is the same as the ambient pressure. Fig. 7 shows the mean radial ventilation rate per cycle $\overline{\dot{m}_{aY}}$ with the amplitude at different frequencies for the 2-D annulus flow.

Fig. 8 shows the temperature contour plots in the air layer annulus for $\xi = 0.8$ and $f = 25$ rpm ($\tau = 2.4$ s) at

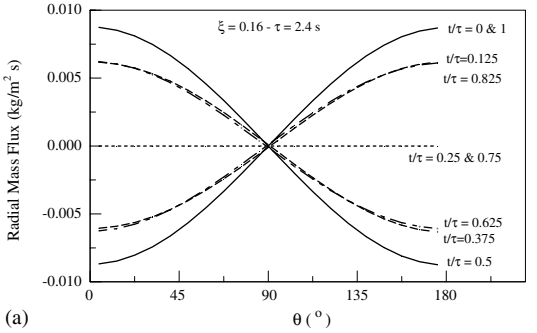

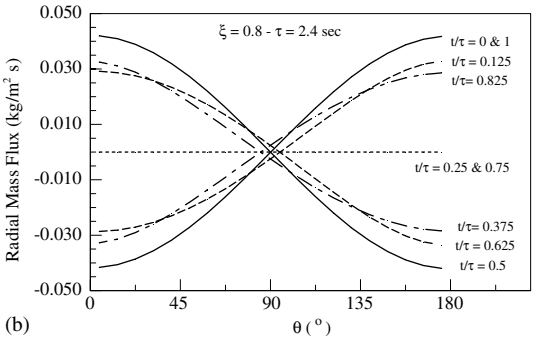

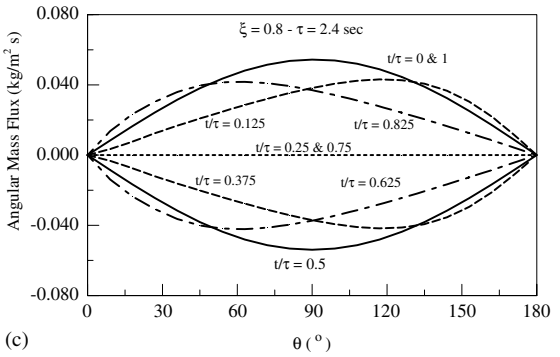

Fig. 5. (a–c) shows the angular variation of (a) the radial ventilation flux at $\zeta = 0.16$; (b) the radial ventilation flux at $\zeta = 0.8$; and (c) the angular internal flow at $\zeta = 0.8$ of the air in the annulus for different times in the motion cycle at $f = 25$ rpm, $Y_m = 38.1$ mm, $L = 50$ cm, $R_f = 7.56$ cm, $R_s = 3.75$ cm, and $C_D = 1$.

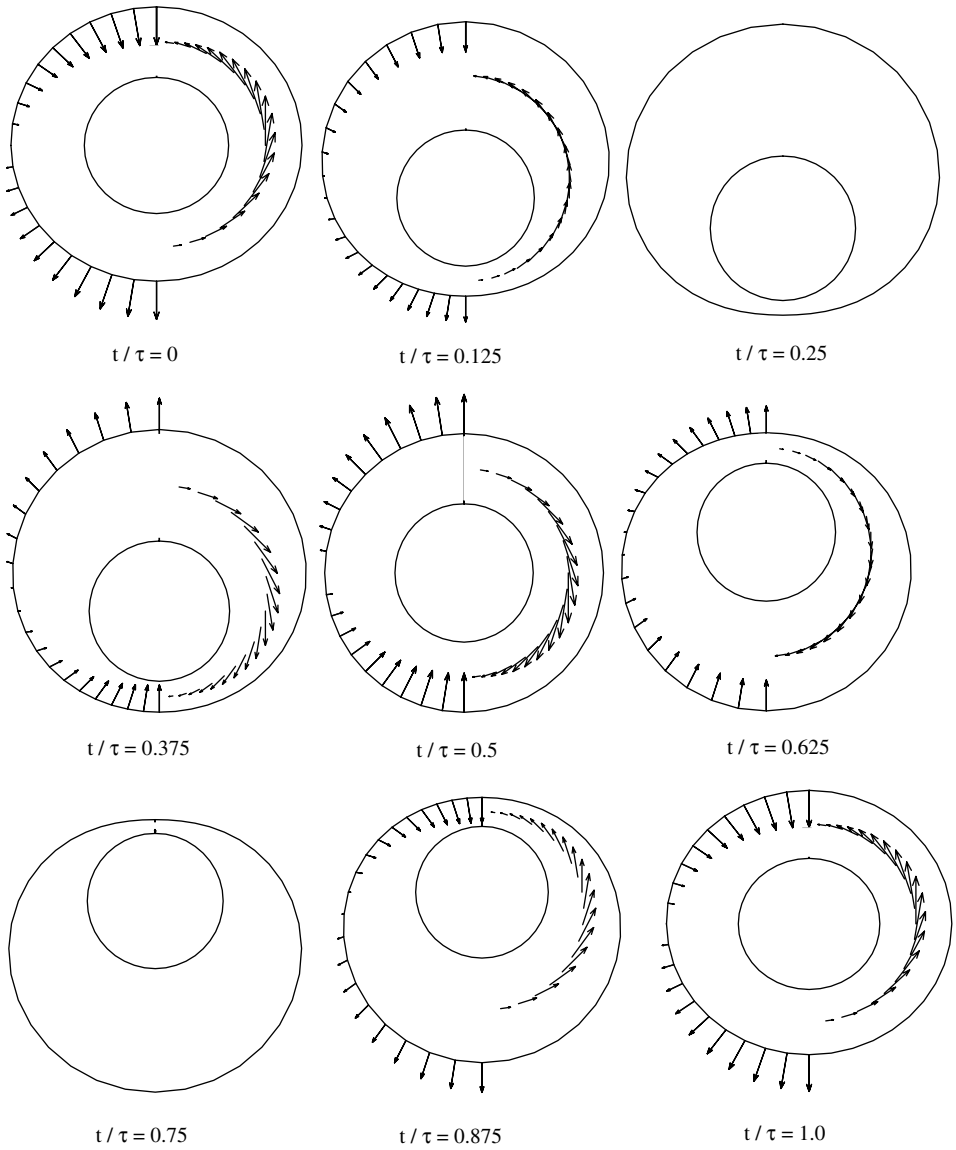

Fig. 6. Vector plot of the angular and radial air layer mass fluxes during one cycle at $\xi = 0.8$ and $f = 25$ rpm ($\tau = 2.4$ s).

different times of the cycle. The hot and cold regions in the annulus are a direct effect of low and high radial ventilation rates, respectively. The temperature varies from 31.44 °C to 34.34 °C. The minimum temperature is at $\theta = 0°$ and $\theta = 180°$ where high radial ventilation rates occur during the motion. The maximum temperatures in the air layer occur around $\theta = 90°$ where minimal radial ventilation exists. When the inner cylinder (arm) is moving in the downward direction, radial air penetration comes from the environment through the fabric air voids causing lower temperatures in that region. During upward motion of the arm, a gradual heating of the upper half region occurs due to the hot air adjacent to the skin penetrating the fabric void and leaving the domain with a gradual cooling in the lower side as the ambient air now penetrates the lower section.

5.3. Open apertures 3-D annular system analysis

Introducing an aperture to the arm will induce air renewal in the axial direction through the opening, in addition to the radial direction renewal. Fig. 9(a)–(c) presents a plot of (a) the mean ventilation rate at the opening $\bar{\dot{m}}_o$ vs. the amplitude ratio at different frequencies of motion; (b) the flow rate at the opening vs. time during one period of oscillation at different amplitude

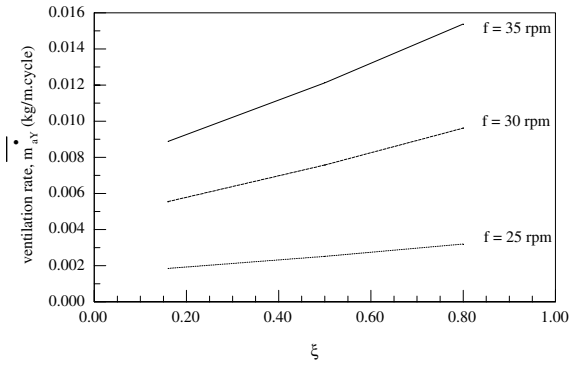

Fig. 7. The variation of the radial ventilation rate $\dot{m}_{aY}$ with the amplitude ratio at different frequencies of $f = 25$, 30, and 35 rpm for 2-D flow of the annulus.

ratios, (c) the axial variation of the time and θ-space-averaged radial flow rate at different amplitude ratios for $f = 25$ rpm. As the amplitude ratio increases the air renewal through the opening increases (Fig. 9(a)). Conversely, as the frequency increases the ventilation rate through opening decreases. As the oscillation amplitude increases, a delay takes place of the time at which the peak ventilation rates take place during the cycle (Fig. 9(b)). It is clear from Fig. 9(c) that at the opening ($x = 0$), the radial ventilation rate approaches zero and a high gradient of radial flow rate occurs within the first 10% of the opening. For most of the domain interior, negligible axial flow exists and the radial flow rate is constant.

The temperature of the air layer annulus is calculated at the opening at $f = 25$ rpm and $\zeta = 0.16$ and the

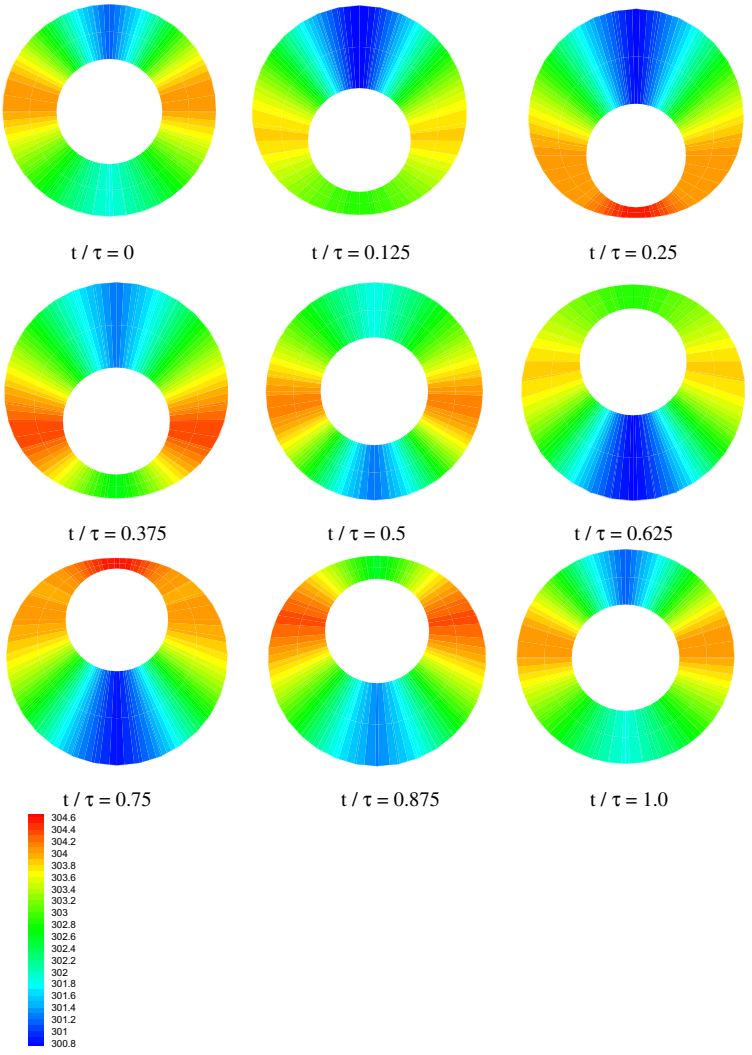

Fig. 8. The temperature contour plots in the air layer annulus for $\xi = 0.8$ and $f = 25$ rpm ($\tau = 2.4$ s) at different times of the cycle.

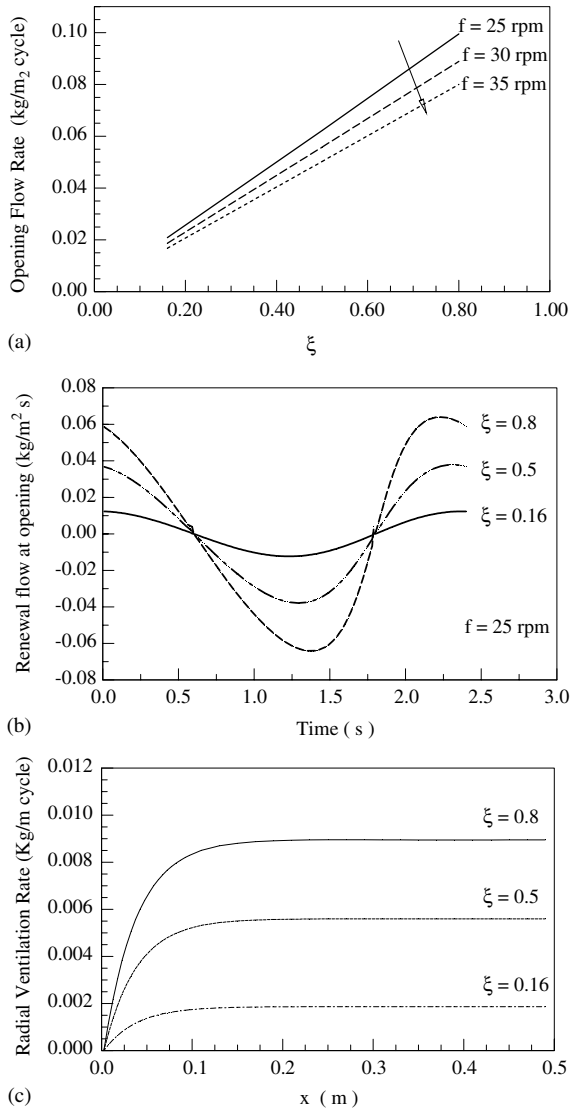

Fig. 9. (a–c) A plot of (a) the mean ventilation rate at the opening $\dot{m}_o$ vs. the amplitude ratio at different frequencies of motion; (b) the flow rate at the opening vs. time during one period of oscillation at different amplitude ratios, (c) the axial variation of the time and θ-space-averaged radial flow rate at different amplitude ratios for $f = 25$ rpm.

temperature is found to vary from 25.34 °C to 32.84 °C. The maximum air temperature is reached around $\theta = \pi/2$ as expected because the air renewal rate is minimum in that region. The maximum spatial temperature difference during the cycle at the opening is around 7.5 K compared to 3.1 K at the closed end. The presence of the opening has actually reduced the cooling effect on the internal air layer and consequently will reduce the sensible and latent heat losses. Fig. 10(a) and (b) show the 3-D ventilation model predictions and the planar

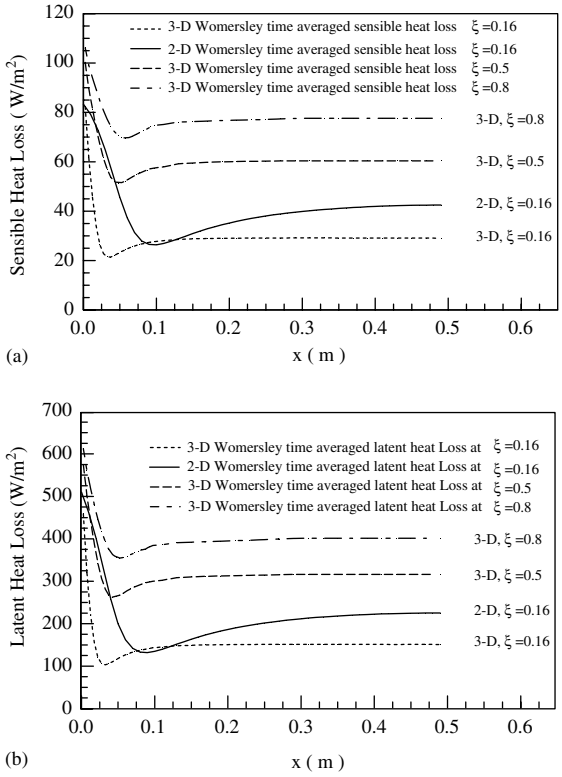

Fig. 10. (a,b) The 3-D ventilation model predictions and the planar 2-D model [2] of (a) time-averaged sensible heat loss and (b) time-averaged latent heat losses in W/m^2 as a function of x at $f = 25$ rpm and $\zeta = 0.16$, 0.5 and 0.8.

2-D model [2] of (a) time-averaged sensible heat loss and (b) time-averaged latent heat losses in W/m^2 as a function of x at $f = 25$ rpm and $\zeta = 0.16$, 0.5 and 0.8. The heat loss increases as the amplitude is increased. In addition, the heat losses are higher at the boundary open to atmosphere because of the big difference between the temperature and humidity ratio between room conditions and the skin condition. The time and space-averaged total heat loss of the 2-D planar ventilation model [2] of parallel air flow in a channel with an upper moving fabric boundary and in presence of open aperture for $f = 25$ rpm was reported as 247.04 W/m^2 compared with 180.44 W/m^2 for the current 3-D open aperture model that include the effect of angular motion. The decrease in heat loss by 27% is due to the angular flow rate that reduces the radial (normal to the fabric) ventilation compared to the 2-D normal/axial ventilation model. Table 1 presents the total sensible and latent heat losses determined at different amplitude ratios and frequencies. Open aperture clothing ventilation system induces less heat loss from the closed aperture clothing ventilation system. At higher frequencies, the effect of the opening on the heat loss is reduced. The results show

Table 1
The time-space averaged sensible and latent heat losses at various ventilation frequencies of the fabric and the corresponding heat losses for closed and open aperture systems

Amplitude ratio ξ	Frequency f (rpm)	Sensible heat loss (W/m^2)		Latent heat loss (W/m^2)	
		Closed apertures (2-D flow radial and angular)	Open aperture (3-D flow)	Closed apertures (2-D flow radial and angular)	Open aperture (3-D flow)
0.16	25	29.45	29.14	152.13	151.30
	30	36.20	36.02	189.40	189.20
	35	42.50	42.13	223.12	222.80
0.5	25	60.58	59.80	317.24	316.20
	30	71.650	68.90	371.23	368.55
	35	84.86	83.70	445.40	443.80
0.8	25	77.63	77.70	402.15	400.90
	30	87.88	86.58	450.60	447.90
	35	95.50	94.80	485.60	483.60

that the presence of the opening has resulted in lower sensible and latent heat loss than the 2-D model representing closed apertures system. The percentage drop in total heat loss due to open aperture is however, less than 1% at the ventilation frequencies considered of 25, 30, and 35 rpm, respectively. These results are consistent with published experimental data of Lotens [3,21,22] and Danielsson [4]. Lotens has reported experimental measurements of the internal air layer evaporative resistance at the skin and in the internal air layer as a function of open or closed apertures and walking speed for high air permeable clothing ensemble made of cotton fabric. He noticed that the resistance to vapor transfer with closed and open apertures are not very different regardless of the outside air velocity. His results show that vapor resistance from the body at zero walking speed and 0.2 m/s wind is slightly higher for closed aperture than for open aperture. However, as walking speed is increased to 0.694 m/s and 1.388 m/s, the evaporative resistance at the skin and in the internal air layer at the same wind speed of 0.2 m/s, decreased by 1.4% and 7.6%, respectively. Similar results have been reported by Danielsson [4] on higher heat loss and higher internal convective coefficients for closed aperture clothing over various body parts as compared to respective values for open aperture clothing at walking conditions. It is clear that for long domains, the presence of the openings will only have a local effect close to the boundary, while at the same time reducing the air renewal flow rate by normal ventilation due to reduced pressure difference through the fabric between the internal layer and the environment.

6. Conclusions

The coupled convection heat and moisture exchange within the clothing system subject to sinusoidal air layer thickness variation about a fixed mean is theoretically modeled to predict the fabric temperature and the transient conditions of the air layer located between the outer fabric and the inner cylindrical skin. The developed mathematical model is based on Womersley flow for the axial and angular flow directions and uses a three-node adsorption ventilation model for the fabric in the radial airflow direction. The predicted ventilation flow rates agree well with experimental measurements of total renewal rates for closed and open aperture. The agreement improves at higher frequencies of ventilation.

The developed model of the 3-D internal air layer flow motion and the resulting flow rates in 3-directions brings results of heat loss closer to the experimental findings of Lotens [3] that show slight reduction in heat loss for open aperture of highly permeable clothing.

The current model approach is novel in its consideration of the periodic nature of air motion in the trapped layer between skin and fabric from first principles that capture all the physical parameters of the system. The model provides an effective and fast method of providing solution at low computational cost. This make the model attractive for integration with human body thermal models to better predict human response under dynamic conditions. The 3-D motion within the air layer and its interaction with the ambient air through the fabric and the aperture is a complex basic problem. The introduction of the Womersley flow in the axial and angular directions has reduced the complexity of the solution and predicts realistic mass flow rate through the apertures. In long domains, the effect of the aperture is localized. In conclusion the model is not computationally expensive since a two independent 1-D models in the polar and axial directions are used, in additions to a lumped model in the radial direction. The results produced captured the physics of the flow and accurately predicted the heat loss from the body.

Acknowledgements

The authors would like to acknowledge the financial support of the University Research Board of the American University of Beirut. The environmental chamber lab facility is supported by the American School and Hospital Aid (ASHA) grant AUB-FEA-793.

References

[1] K. Ghali, N. Ghaddar, B. Jones, Empirical evaluation of convective heat and moisture transport coefficients in porous cotton medium, J. Heat Transfer 124 (3) (2002) 530–537.

[2] N. Ghaddar, K. Ghali, J. Harathani, Inertia effects on the modulated air layer heat and moisture transport from clothing with open aperture, in: Proceedings of the 2004 ASME Heat Transfer Heat Transfer/Fluids Engineering Summer Conference, paper number HT-FED2004-56099, Charlotte, North Carolina, USA, 2004.

[3] W.A. Lotens, Heat transfer from humans wearing clothing, Ph.D. thesis, TNO Institute for Perception, Soesterberg, The Netherlands, 1993, pp. 34–37.

[4] U. Danielsson, Convection coefficients in clothing air layers, Ph.D. thesis, The Royal Institute of Technology, Stockholm, 1993.

[5] G. Havenith, R. Heus, W.A. Lotens, Resultant clothing insulation: a function of body movement, posture, wind clothing fit and ensemble thickness, Ergonomics 33 (1) (1990) 67–84.

[6] G. Havenith, R. Heus, W.A. Lotens, Clothing ventilation, vapor resistance and permeability index: changes due to posture, movement, and wind, Ergonomics 33 (8) (1990) 989–1005.

[7] B.W. Jones, M. Ito, E.A. McCullough, Transient thermal response systems, in: Proceedings of the International Conference on Environmental Ergonomics, Austin, TX, 1990, pp. 66–67.

[8] B.W. Jones, E.A. McCullough, Computer modeling for estimation of clothing insulation, in: Proceedings of CLIMA 2000, World Congress on Heating, Ventilating, and Air Conditioning, Copenhagen, Denmark, vol. 4, 1985, pp. 1–5.

[9] Y. LI, B.V. Holcombe, Mathematical simulation of heat and moisture transfer in a human-clothing-environment system, Text. Res. J. 68 (6) (1998) 389–397.

[10] K. Ghali, N. Ghaddar, B. Jones, Multi-layer three-node model of convective transport within cotton fibrous medium, J. Porous Media 5 (1) (2002) 17–31.

[11] K. Ghali, N. Ghaddar, B. Jones, Modeling of heat and moisture transport by periodic ventilation of thin cotton fibrous media, Int. J. Heat Mass Transfer 45 (2002) 3703–3714.

[12] N. Ghaddar, K. Ghali, B. Jones, Integrated human-clothing system model for estimating the effect of walking on clothing insulation, Int. J. Therm. Sci. 42 (6) (2003) 605–619.

[13] K. Ghali, N. Ghaddar, J. Harathani, Two dimensional clothing ventilation model for a walking human, in: Proceedings of the International Conference on Thermal Engineering: Theory and Applications. Paper No. ICTEA-TF1-03, Beirut-Lebanon, May 31–June 4, 2004.

[14] J.R. Womersley, Oscillatory motion of viscous liquid in thin-walled elastic tube: i. The linear approximation for long waves, Philos. Mag. 46 (1955) 199–221.

[15] J.R. Womersley, An elastic tube theory of pulse transmission and oscillatory flow in mammalian arteries, Aeronautical Research Laboratory, WADC Technical Report TR 1957, pp. 56–614.

[16] L.W. Lamoreux, Kinematic measurements in the study of human walking, Bull. Prosth. Res. (1971) 3–86.

[17] American Society for Testing and Materials. ASTM D737-75, Standard Test Method for Air Permeability of Textile Fabrics, (IBR) approved 1983.

[18] A.G. Straatman, R.E. Khayat, E. Haj-Qasem, D.A. Steinman, On the hydrodynamic stability of pulsatile flow in a plane channel, Phys. Fluids 14 (6) (2002) 1938–1944.

[19] D.J. Acheson, Elementary Fluid Dynamics, fourth ed., Clarendobn Press, New York, 1990.

[20] R.W. Hyland, A. Wexler, Formulations for the Thermodynamic Properties of the Saturated Phases of H_2O from 173.15 K to 473.15 K, ASHRAE Trans. 89 (2A) (1983) 500–519.

[21] W.A. Lotens, G. Havenith, Calculation of clothing insulation and vapor resistance, Ergonomics 34 (2) (1991) 233–254.

[22] W.A. Lotens, G. Havenith, Effects of moisture absorption in clothing on the human heat balance, Ergonomics 38 (1995) 1092–1113.